Keywords
Chronic obstructive pulmonary disease (COPD); Ellagic acid; Phosphodiesterase-4 (PDE4); Molecular docking; Molecular dynamics simulation; MM-GBSA; Anti-inflammatory activity; cAMP

Authors
Subhajit Dutta[1]
Research Scholar, TIFAC CORE in Herbal Drugs, Department of Pharmacognosy and Phytopharmacy, JSS College of Pharmacy, JSS Academy of Higher Education and Research, Ooty - 643001, India.
Email: subhajitdutta174@gmail.com
ORCID ID: 0009-0007-6257-3559

Shanmugam Ramaswamy[2*]
Associate Professor, Coordinator, TIFAC CORE in Herbal Drugs, Department of Pharmacognosy and Phytopharmacy, JSS College of Pharmacy, JSS Academy of Higher Education and Research, Ooty- 643001, Tamil Nadu, India.
E-mail: shanmugamr@jssuni.edu.in
ORCID ID: 0000-0002-7972-3425

L Priyanka Dwarampudi[3]
Assistant Professor and Head, Department of Pharmacognosy and Phytopharmacy, JSS College of Pharmacy, JSS Academy of Higher Education and Research, Ooty- 643001, Tamil Nadu, India,
E-mail: lalithapriyanka25@jssuni.edu.in

S P Dhanabal[4]
Principal and Professor, Department of Pharmacognosy and Phytopharmacy, JSS College of Pharmacy, JSS Academy of Higher Education and Research, Ooty- 643001, Tamil Nadu, India.
Email: spdhanabal@jssuni.edu.in

Sagarkanta Mohanty[5]
Research Scholar, Department of Pharmaceutical Chemistry, JSS College of Pharmacy, JSS Academy of Higher Education and Research, Ooty- 643001, Tamil Nadu, India.
Email: sagarkantamohanty2001@gmail.com

Srikanth Jupudi[6]
Department of Pharmaceutical Chemistry, JSS College of Pharmacy, JSS Academy of Higher Education and Research, Ooty- 643001, Tamil Nadu, India.
Email: sjphd@jssuni.edu.in

Received:27-06-2026
Revised:30-07-2026
Accepted:05-08-2026
Doi:10.1922/ejprd.v34i7s.1718

Integrated Computational and Experimental Evaluation of Ellagic Acid as a Natural Phosphodiesterase-4 Inhibitor for the Management of Chronic Obstructive Pulmonary Disease

Abstract

Background: Chronic obstructive pulmonary disease (COPD) is a chronic inflammatory disease of the respiratory tract; it causes considerable morbidity and mortality worldwide. Phosphodiesterase-4 (PDE4) is a validated target for drug development, and PDE4 inhibitors increase intracellular cAMP and inhibit inflammatory signals. However, the adverse effects of the PDE4 inhibitors currently available (including roflumilast) have restricted their clinical use, which makes natural PDE4 inhibitors with fewer adverse effects more desirable.

Methods: An integrated computational and experimental approach was used to discover natural PDE4 inhibitors from an Ayurvedic phytoconstituent library, which consisted of 250 phytoconstituents. The prioritized compounds after physicochemical filtering and pharmacophore-based virtual screening were then docked into the catalytic domain of PDE4 (PDB ID: 4WCU) and subsequently the binding free energies of these selected chemicals were computed using MM-GBSA approach. The prioritized compounds were also evaluated for their ADMET, toxicity and 200_ns MD simulation. Ellagic acid was chosen as the lead compound and further tested in the in vitro antioxidant (DPPH) and BEAS-2B cell viability (SRB), pro-inflammatory cytokine (TNF-α, IL-6, and IL-1β) and nitric oxide inhibition and intracellular cAMP assays.

Results: Molecular docking revealed that Ellagic acid had a Glide XP score of −9.262 kcal/mol and MM-GBSA binding free energy of −72.56 kcal/mol with the catalytic pocket of PDE4 and showed stable hydrogen bonding with some key catalytic residues such as TYR159, ASP318, GLN369 and PHE372 for favourable binding. Molecular dynamics simulations showed that the PDE4–Ellagic acid complex exhibited minimal conformational changes of the protein and ligand during the 200 ns simulation and that the protein–ligand interactions were maintained. In silico ADMET and toxicity prediction indicated acceptable pharmacokinetic properties, and a favourable predicted safety profile. In vitro, Ellagic acid had strong antioxidant activity (DPPH $IC_{50} \approx 38$ µg/mL), low cytotoxicity to BEAS-2B cells ($IC_{50} = 735.4$ µg/mL) and significantly reduced the production of TNF-α, IL-6, IL-1β and nitric oxide in LPS stimulated RAW264.7 macrophages, and restored intracellular cAMP levels in inflamed BEAS-2B cells, supporting modulation of the PDE4/cAMP signaling pathway.

Conclusions: The combination of computational and experimental results shows that Ellagic acid is a promising natural lead compound for PDE4 targeting therapy for COPD. All these properties indicate that it is highly favourable for binding, stable molecular interactions, an acceptable predicted pharmacokinetic profile, potent antioxidant activity, anti-inflammatory properties and the ability to restore intracellular cAMP, which indicate further investigation and preclinical development. However, biochemical PDE4 enzyme inhibition assays and in vivo efficacy assays need to be undertaken to verify its therapeutic potential and mechanism of action.

ejprd.org - Published by Riset Publication Services LLC

Graphical Abstract

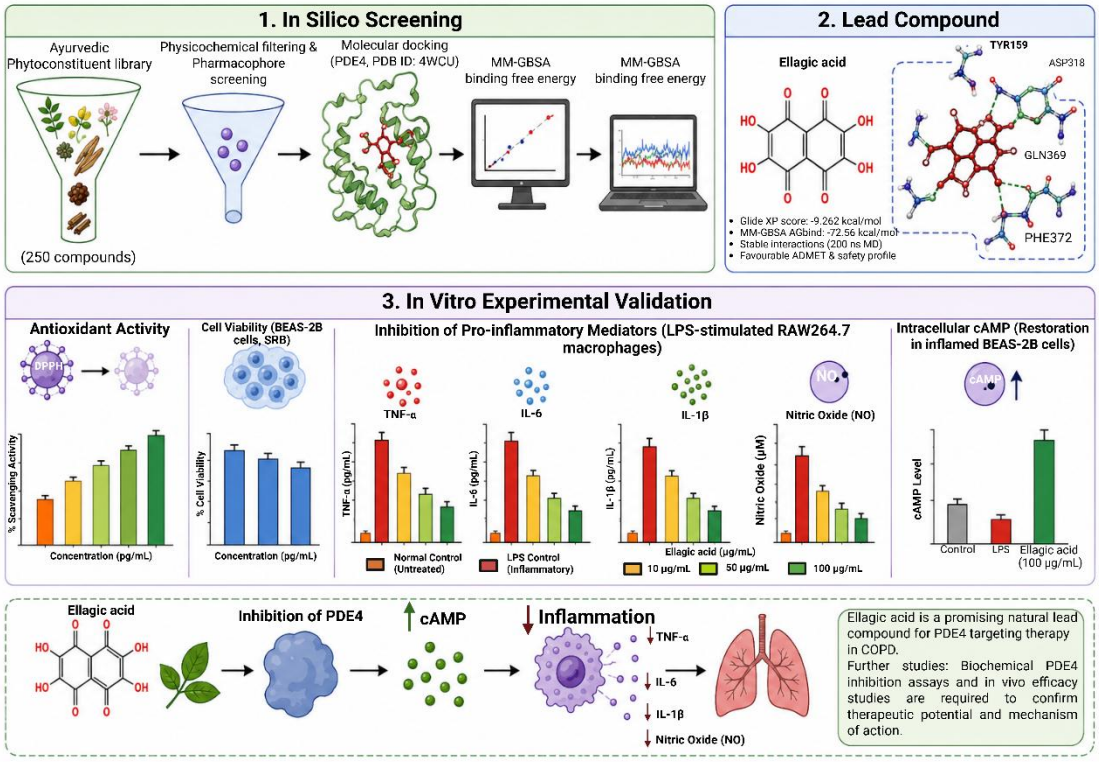

INTRODUCTION

The superfamily of enzymes known as phosphodiesterases (PDEs) degrades the second messengers cAMP and cGMP, thereby controlling many physiological functions. The isoforms of PDE4 that are cAMP selective play a very important role in the control of immunological and inflammatory reactions. PDE4 overactivation is involved in chronic inflammatory diseases [1]. In fact, selective PDE4 inhibitors can increase cAMP levels in the cell to prevent pro-inflammatory cytokines from being produced[2]. So far, there are only two PDE4 inhibitors that have been brought to the clinic: roflumilast (in COPD) and apremilast (in psoriatic arthritis), and both contain a catechol-like motif. The adverse effects of gastrointestinal and neuropsychiatric nature restrict their clinical utility, and the need to identify new PDE4 inhibitors with different scaffolds and a better therapeutic index is imperative. Specifically, the non-catechol natural compounds with a structurally diverse nature can overcome the drawbacks of existing medicines[3].

A search towards natural PDE4 inhibitors has been concerted over the last few years. Indicatively, resveratrol (a grape stilbene) was demonstrated to inhibit PDE3 and PDE4 as well as mediate anti-aging. Non-aromatic PDE4 inhibitors were also characterized by our group as marine and plant-derived: a new prostaglandin derivative from coral and toddacoumalone Toddalia asiatica[4]. In more recent times, powerful PDE4 inhibitors (selaginpulvilins A-L) were discovered in Selaginella pulvinata and had low nanomolar values in terms of IC50. One such fluorescent inhibitor of PDE4D was the crystal structure (PDB 5WQA) that showed an unusual binding mode. These findings show that natural compounds may be able to produce novel PDE4 ligands, which are frequently too complex to co-crystallize, and thus require computational docking to provide mechanistic information[5].

With the accessible structural information (e.g. PDE4D structures PDB ID 4WCU, 5WQA), an in-silico screening is a valuable approach that can be used to suggest new inhibitors. Thus, we use the method of molecular docking of Ellagic acid into the PDE4 active site (4WCU) to predict the binding conformation and the affinity. The PDB model (4WCU) of the human PDE4D in the presence of a small-molecule inhibitor (LEO 29102) is a high-resolution (2.35 A) model to design around structure[6,7].

Ellagic acid (EA) is suggested as the compound of interest (replacement). EA is a naturally occurring polyphenolic dilactone (C 14H 6O 8, MW 302.20 g/mol) which is a hydrolysate of ellagitannins[8]. Estructurally, EA is a fused ring compound that has four phenolic OH groups; it is highly polar and is virtually insoluble in water. In spite of low bioavailability, EA has been touted to have a wide spectrum of bioactivity. It is rich in pomegranates, berries and nuts and is a powerful antioxidant and anti-inflammatory[9]. Several studies have found that EA prevents oxidative stress and inflammatory signal transduction: e.g., EA prevents oxidized-LDL-induced inflammatory response in endothelial cells, and prevents cytokines causing inflammation from being released in an animal model of vascular disease[10]. It has also been demonstrated that EA has vasodilatory effects through the NO/cAMP signaling pathways. Some literature has shown that EA increased intracellular levels of cAMP in smooth muscle and synergized with the PDE4 inhibitor rolipram. This implies that EA can indirectly tune PDE4-associated pathways, but has not been directly reported to interact with the enzyme[11].

In this light, we will hypothesise that EA, per se, can bind to and inhibit PDE4. The hypothesis is that EA, based on its polyphenolic structure and capacity to stimulate cAMP, might be inserted into the PDE4 active site and inhibit cAMP hydrolysis. This will be tested by molecular docking to determine the binding mode of EA in PDE4 (4WCU), and compare it to the known inhibitor (LEO 29102) and Roflumilast. The drug-like properties of EA will also be taken into consideration[12]. EA is not very lipophilic (logP = -0.2) and has a number of hydrogen bond acceptors/donors (4 H-bond donors, 8 acceptors). These properties are in opposition to those of common PDE4 inhibitors (usually more hydrophobic), and may affect binding and ADMET. The EA ADMET profile has been highly researched: it is non-toxic in dietary amounts and has GRAS status, but has poor solubility, which restricts its bioavailability. However, the safety and oral bioactivity of EA have been established, which is why it should be investigated regarding its pharmacological potential[13].

It is on this basis that the current study adopted an integrated approach of computation and experimental design in the discovery of Ellagic acid as a potential natural inhibitor of phosphodiesterase-4 (PDE4) to manage COPD. Ellagic acid was first chosen in a virtual screening workflow, then molecular docking with the catalytic domain of PDE4 (PDB ID: 4WCU) was performed to determine the interaction of the drug and its inhibitory abilities[14]. The stability of the Ellagic acid PDE4 complex was then assessed using molecular dynamics simulations, and binding affinity was ascertained by calculating binding free energy (MM-GBSA), electronic characteristics and molecular reactivity. Moreover, physicochemical characteristics, pharmacochemical behavior, drug-like, and toxicity profiles were fully evaluated with the aid of in silico ADMET predictive tools[15,16]. Lastly, the computational results were confirmed by exploring the in vitro antioxidant, anti-inflammatory, Nitric Oxide inhibitory assay and cAMP level measurement assay to determine the therapeutic prospects of Ellagic acid as a new natural PDE4 inhibitor. This multi-scale methodology, in combination, gives mechanistic information about the interaction between Ellagic acid and PDE4 and about its potential to serve as a lead molecule to develop safer and more effective therapeutic interventions against COPD.

2. Methodology

2.1 High-Throughput Virtual Screening and Ligand Preparation

An Ayurvedic phytoconstituent library containing 250 phytoconstituents listed in the Ayurvedic Formulary of India was compiled in order to discover possible natural phosphodiesterase-4 (PDE4) inhibitors. Before the virtual screening, physicochemical filtering of the compound library according to the Rule of Five by Lipinski, as well as the elimination of compounds with highly reactive or chemically unstable functional groups, was performed to obtain 150 structurally diverse drug-like compounds to be evaluated by computational methods. The catalytic domain of the human PDE4 crystal structure with PDB ID: 4WCU and the ligand library were prepared and used the crystal structure obtained from the RCSB Protein Data Bank (https://www.rcsb.org/) to screen them against one another[17–20]. The active-site region has been chosen according to the co-crystallized ligand's coordinates, and all compounds were first put through an initial virtual screening workflow[21,22]. The ranking of the candidate molecules was done according to the Glide docking score, the binding orientation, and contact between the potential compounds and the essential PDE4 catalytic pocket residues[23]. The most promising compounds with good binding affinity and interaction characteristics were shortlisted to carry out further computational studies as indicated in Table 1.

The Epik module of the Schrödinger Suite was utilized to produce up to 20 energetically accessible conformers per compound within the physiological pH range of 7.0 + 2.0 to thoroughly explore the flexibility of the conformations of each ligand. The ionization states and associated tautomeric forms were predicted and the energetically unfavourable tautomers were not analyzed further. After conformational preparation, a virtual screening protocol based on a pharmacophore was carried out with the Phase module[24,25]. Ligands were screened based on the Phase Screen Score, a combination of vector alignment, volume overlap and RMSD-based site matching to determine the strength of the pharmacophore. The compounds with a Phase Screen Score of 1.5 or higher were viewed as potential hits and were chosen to be studied in molecular docking[26,27]. Lastly, the LigPrep module was used to optimize three-dimensional geometries of all shortlisted ligands, assign protonation states, correct where necessary, correct stereochemistry, and to minimize the energy with the OPLS4 force field. The ligand structures were then prepared, and precision molecular docking was performed on the PDE4 catalytic pocket using the prepared ligand structures to determine which natural inhibitor was the most promising to further validate using computational and experimental methods.

2.2 Protein Preparation

The Protein Data Bank (RCSB PDB; https://www.rcsb.org) provided the 3-D X-ray crystal structure of human phosphodiesterase-4 (PDE4) in complex with a co-crystallized inhibitor (PDB ID: 4WCU), which served as the receptor model for all molecular docking, molecular dynamics (MD) simulation, and binding free energy calculations[28,29]. The chosen crystal structure has a resolution of 2.35 A which offers a high-quality structural backbone with a defined catalytic binding pocket for structure-based virtual screening and ligand-binding studies. To achieve an energetically optimized receptor structure, which can be used in computational analyses, protein preparation was done with the Protein Preparation Wizard of the Schrödinger Suite 2025-4[30]. To remove all non-essential solvent molecules, all the crystallographic water molecules outside of the catalytic region, which were involved in fewer than three hydrogen-bond interactions, were removed first. The protein structure was then modified to represent physiological parameters (pH 7.0 + 0.2) by adding hydrogen atoms, assigning bond ordering, and adjusting the protonation states of ionizable residues[31]. In the cases of missing side chains, these were rebuilt with the Prime module, then the hydrogen-

bonding network was optimized to achieve the correct orientations of the polar residues. Lastly, the minimization of the energy restrained with the OPLS4 force field was continued until the RMSD of the heavy atoms became less than 0.3 Å to minimize the steric clashes without altering the geometry of the crystal observed in the experiment[32–34]. A structural examination of the receptor so made showed that there were only a few unresolved loop and side-chain regions that were found on peripheral surfaces that were exposed to solvents. Notably, no gaps in the sequence or structural discontinuities were observed in or near the catalytic binding pocket, thereby obviating the need to use homology modelling and the subsequent reconstruction of the structure on a large scale. Therefore, localized refinements were the only refinements done in the normal protein preparation workflow to refine the stereochemical quality of the receptor before receptor-grid generation[35,36].

The Receptor Grid Generation module of Schrödinger was used to generate the molecular docking receptor grid, with the grid box centered on the co-crystallized inhibitor's binding site. The docking grid was delimited to cover the entire catalytic cavity, including the important amino acid residues HIS160, TYR159, ASP318, TYR329, GLN369, PHE372, THR333 and ASN395 that are important in ligand recognition and PDE4 inhibition. The positions of the attached ligand in the structure of the crystal (PDB ID: 4WCU) were used to create the grid as the centroid to make sure that the biologically relevant active site is represented in all the subsequent molecular docking and computational studies[37,38].

2.3 Molecular Docking Studies

The affinity for binding and interaction pattern of the selected phytoconstituents to the catalytic domain of the human PDE4 were ascertained using molecular docking assays. The PDE4 X-ray crystal structure in the presence of an inhibitor (PDB ID: 4WCU) that has been co-crystallized acquired from the Protein Data Bank (https://www.rcsb.org/). The chosen structure is one with a high crystallographic resolution (2.35 A) and a strong co-crystallized inhibitor with an IC50 of 3 nM, and will thus be a useful structure template in structure-based drug discovery[39]. The receptor structure had been prepared as outlined in Section 2.2, which was further used to generate receptor grids and conduct molecular docking analyses. Protein Preparation Wizard. During the preparation procedure, the side-chain atoms and missing hydrogen atoms were added, and crystallographic water molecules with less than three hydrogen bonds were removed[40]. The ionizable residues were protonated at physiological pH (7.0 ± 0.2), and restrained energy minimization of the OPLS4 force field was used until convergence of the heavy atoms to a root-mean-square deviation (RMSD) of 0.3 A was achieved, to obtain a geometrically optimized receptor that can be used in docking calculations. After virtual screening based on pharmacophore, shortlisting of about 8, 500 compounds was performed, followed by a hierarchical molecular docking workflow with the Glide module of Schrodinger Suite[41,42]. To begin with, Standard Precision (SP) docking was carried out to selectively remove those ligands that do not strongly interact with the catalytic site and to rank the compounds with good binding orientations and interactions in the PDE4 catalytic site. According to Glide GScore, binding orientation, contact with key catalytic residues and the quality of docking, the top ligands of the SP stage were further selected to be subjected to Extra Precision (XP) docking, which further assesses the binding affinity and molecular recognition of the ligand. The end docking poses were categorized based on the value of Glide GScore, Glide Energy and Glide Emodel[43,44]. In addition to docking scores, each ligand's interaction profile with PDE4's essential catalytic residues was carefully examined to ascertain if stable hydrogen bonds, hydrophobic contacts, π-stacking interactions and other non-covalent interactions that might help stabilize the ligand in the active site. The top-ranking ligand conformations using XP docking were further used in MM-GBSA binding free energy and molecular dynamics simulations, among other downstream computational analysis to thoroughly assess their inhibitory capability against PDE4[45,46].

2.4 MM-GBSA Calculation

The Prime Molecular Mechanics-Generalized Born Surface Area (MM-GBSA) module of Schrödinger Suite 2025-4 was used to calculate the binding free energy of the selected ligands with phosphodiesterase-4 (PDE4) for a more precise approximation of the binding affinity of the selected ligands[47,48]. The top docking conformations of the Glide XP docking were used to carry out the MM-GBSA analysis to further assess the thermodynamic stability of the ligand in the catalytic binding pocket of PDE4. All calculations were done using the OPLS4 force field, and the implicit solvent model VSGB 2.1 [49]. Each protein–ligand complex was locally energy-minimized keeping the backbone of the whole receptor in a fixed conformation to preserve the crystallographic geometry and the energy of each complex was calculated. To obtain the binding free energy (ΔGbind), molecular mechanics energies were then combined with the generalized Born electrostatic solvation and solvent-accessible surface area (SASA) to obtain the binding free energy[50]. Besides the overall binding free energy, decomposition of the energies in MM-GBSA was performed to understand the contribution of individual energy terms in the recognition and stabilisation of the ligand in the active site. These interactions were coulombic interactions, the hydrogen-bonding energy, van der Waals interactions, lipophilic interactions and solvation energy. Compounds with the most desirable negative values of ΔGbind along with stable interaction patterns were chosen as potential lead candidates and further underwent molecular dynamics simulations and experimental validation[51,52].

2.5 Toxicity Profile

Prioritized compounds' toxicity profiles were predicted using the ProTox-3.0 web server (https://tox.charite.de/protox3/), which is an in-silico toxicity prediction platform. For each chemical compound (with experimentally validated toxicological data) and reliable information source, the safety profile of these compounds was estimated using machine learning algorithms as well. Computational toxicity prediction, through this approach, can begin to focus on early identification of potential toxicity problems and diminish

the need for large-scale experimental toxicity studies. The toxicity was predicted (median lethal dose, LD 50), and the toxicity has been classified along with all its organ-specific and systemic toxicity effects that include hepatotoxicity, neurotoxicity, nephrotoxicity, respiratory toxicity, cardiotoxicity, cytotoxic effects, blood brain barrier (BBB) toxicity, mutagenicity, immunotoxicity, and carcinogenicity. The toxicity profiles made were further merged with the ADMET results and allowed for a holistic view of the safety profiles of the selected lead compounds before further computational & biological studies[53].

2.6 Molecular Dynamics Simulation

Molecular dynamics (MD) simulations were done in the Desmond Molecular Dynamics System in Schrodinger Suite 2025-4 in order to study dynamic behaviour and structural stability of the protein-ligand complexes under physiological conditions. The most promising one, PDE4-ellagic acid complexes along with the inert molecule Roflumilast, were simulated, and the OPLS4 force field was used in the simulation protocol. To neutralize all the protein-ligand complexes, the proper number of counter ions (Na+) and explicit water molecules (TIP3P) were added into each system, and then simulations were run in an orthorhombic simulation box. The end solvated system consisted of about 16 649 water molecules; 55 887 atoms and the volume of the simulation box was 1 174 189 A 3. The calculation of short-range van der Waals and Coulombic interactions was done with a cutoff distance of 10 A and long-range electrostatic interactions were done using the Smooth Particle Mesh Ewald (PME) method with an electrostatic tolerance of 1 × 10^-9. After construction of the systems, a standard relaxation protocol (1000 steps of steepest descent, and conjugate-gradient energy minimization) followed by treatment on a gradual equilibration protocol, was applied to all the models before a production simulation was applied[54,55]. The production was done at an isothermal-isobaric (NPT) ensemble, at 1 bar and 300K temperature and pressure for a 200 nm simulation. To ensure a constant temperature, NoséHoover thermostat and pressure with a Martyna-Tobias-Klein barostat were used to control temperature and pressure, respectively. In the trajectory analysis, several pathways have been used to get deep insight into the stability and conformational changes of the protein-ligand complexes, including RMSD, RMSF and protein-ligand interaction profiling, secondary structure element (SSE) analysis, ligand torsional behaviour profiling and ligand centre of mass (CM) motion profiling throughout the time course of the simulation. The most promising compound obtained during the screening process of compounds (highest ranked Ellagic acidPDE4 complex) was chosen for the rest of the molecular dynamics simulation to confirm the dynamic stability of the lead compound that was computationally identified in the catalytic binding pocket of PDE4 under simulated physiological conditions [56–58].

2.7 In Vitro Studies

2.7.1 Antioxidant Activity (DPPH Radical Scavenging Assay)

Antioxidant activity of Ellagic acid was determined by the 2,2-diphenyl-1-picrylhydrazyl (DPPH) radical scavenging assay, which is one of the commonly used assays for free radical scavenging activity of natural substances. An initial DPPH stock solution was prepared in methanol containing 24 mg DPPH in 100 mL, which was well mixed to give a homogeneous solution. The radical scavenging assay was carried out in a 96-well microplate. In brief, 140 µL of freshly prepared DPPH solution was added to 20 µL of Ellagic acid solution at varying concentrations (0, 10, 25, 50, 75, 100, 125, 250 and 500 µg/mL) to produce the test reaction mixture. The control was methanol:140 µL, DPPH solution:20 µL, time:30 min, while all other experimental conditions were kept constant. After incubation, the microplate was stored at room temperature in the dark for 30 min to complete the radical scavenging reaction. The absorbance of each well was then measured at a wavelength of 517 nm with a microplate reader[59,60].

The DPPH radical scavenging activity (RSA) was measured as a percent according to the following formula:

Radical Scavenging Activity (%)=Ac−AsAc×100

where:

Ac = Absorbance of the control

As = Absorbance of the sample

From the dose-response curve, the concentration of Ellagic acid that reduced the DPPH radicals by 50% (IC50) was calculated and served as a measure for antioxidant activity. Each experiment was repeated three times, and results were plotted as mean ± S.D (Standard Deviation).

2.7.2 Cell Viability Assay (Sulforhodamine B Assay)

The cell viability of Ellagic acid in human bronchial epithelial BEAS-2B cells was measured by Sulforhodamine B (SRB) assay performed as reported earlier. Contents with three different concentrations of Ellagic acid (10, 100 and 1000 µg/mL) were chosen for cellular viability and proliferation. In brief, BEAS-2B cells (5×10^3 cells/well) were seeded in 96-well culture plates and grown in 100 µL complete growth medium for 24 h to ensure cell adhesion. After that, 100 µL of the fresh culture medium comprising various concentrations of ellagic acid was fed to the culture and incubated for 72 h under standard cell culture conditions. The culture medium was removed after treatment, and the cells were fixed by adding 150 µL of 10% (w/v) Trichloroacetic Acid (TCA) into each well and incubating at 4°C for 1 h. The TCA solution was removed, and the plates were washed five times with distilled water to remove unbound cellular components and any residual medium. The fixed cells were then submitted to staining with either 70 µL (w/v) Sulforhodamine B (SRB) solution for 10 min at room temperature in the dark. The plates were washed three times with 1% acetic acid to remove excess dye, and then air dried overnight. The protein-bound SRB dye was then solubilized in 150 µL of the solubilizing agent (10 mM Tris base), and the optical density (absorbance) was assessed at 540 nm by using an Omega microplate reader (BMG LABTECH, Ortenberg, Germany). Cell viability was represented as a percentage of untreated control cells, and the IC_{50} value was obtained from the concentration-response curve[61,62].

2.7.3 Anti-inflammatory Activity: Pro-inflammatory Cytokine Assay

Anti-inflammatory effect of Ellagic acid was assessed based on its inhibitory effect on RAW264.7 mouse macrophage cells to produce the pro-inflammatory

cytokines tumor necrosis factor alpha (TNF-α), interleukin-6 (IL-6) and interleukin-1 beta (IL-1β). RAW264.7 cells were cultured in 96-well culture plates at a density of 2 × 10^5 cells/well for 1 h before they adhered. The cells were then exposed to various doses of Ellagic acid, which were then stimulated with lipopolysaccharide (LPS, 0.2 µg/well) to elicit an inflammatory response. Culture medium was added in control wells, and no LPS was stimulated. After 24 h of incubation, the culture supernatants were harvested, and the levels of TNF-alpha, IL-6 and IL-1β were determined by commercially available enzyme-linked immunosorbent assay (ELISA) and were done according to the manufacturer's instructions. These were read at a microplate reader at 450 nm, and the concentration of cytokines was determined from the standard calibration curves[63,64].

2.7.4 Nitric Oxide (NO) Inhibition Assay

The inhibitory activity of Ellagic acid on nitric oxide (NO) production was determined in the LPS-stimulated RAW264.7 macrophages by the modified Griess reaction. RAW264.7 cells were cultured in 96-well plates (2 × 10^5/well) for 4 h to adhere. Then, different concentrations of Ellagic acid (10, 100, and 1000 µg/mL) were used to treat the cells with or without Escherichia coli-derived LPS (1 µg/mL). Cells, unstimulated with LPS (mock), were considered normal controls and cells stimulated with LPS alone were considered positive inflammatory controls. After incubation in 24-well plates for 24 hours at 37°C in a humidified CO_2 incubator with 5% CO_2 and 95% humidity, equal volumes of the culture supernatant and the modified Griess reagent were combined and incubated for 15 minutes at room temperature. It was then measured by a microplate reader at 540 nm absorbance. The production of NO was determined by comparing it with the standard curve made by Sodium nitrite, and the effect of Ellagic acid was expressed in comparison with the LPS-treated control group[65,66].

2.7.5 Intracellular cAMP Level Measurement

To investigate the pharmacological effects of Ellagic acid as a PDE4 inhibitor in an in vitro COPD inflammatory model, the intracellular cyclic adenosine monophosphate (cAMP) levels were quantified. In summary, BEAS-2B cells were cultured under inflammatory conditions similar to COPD-related airway inflammatory conditions and stimulated with LPS (10 µg/mL) for 24 hours. The cells were treated with Ellagic acid (10 µM) under the same culture conditions after LPS stimulation. Cells were harvested and lysed at the end of the treatment period, as per the manufacturer's instructions. The concentration of cAMP then was measured by competitive enzyme-linked immunosorbent assay (ELISA) kit. Absorbance was read in a microplate reader, and the intracellular cAMP was determined by using a standard curve prepared as per the manufacturer's instructions[67,68].

2.8 Statistical Analysis

Data are expressed as means ± standard deviations (SD) of at least three independent experiments. Data were analysed using GraphPad Prism software (version 10.0, GraphPad Software Inc., San Diego, CA, USA). One-way analysis of variance (ANOVA) with Tukey's multiple comparison post hoc test was performed among the experimental groups. Statistically difference was considered significant at a P-value of < 0.05.

3. Results

3.1 Molecular Docking Study

The progressive screening of the compounds through a multistep virtual screening process prioritised the phytoconstituents according to their highest predicted affinity for the phosphodiesterase-4 (PDE4) catalytic domain. The shortlisted compounds were then extensively docked, and binding free energy was estimated using the MM-GBSA approach to identify compounds that may have binding affinity compared to the clinically approved PDE4 inhibitor Roflumilast (CID: 449133). As summarized in Table 1, all prioritized phytoconstituents showed better docking affinity than the reference drug and Glide GScores ranged between −9.173 and −12.914 kcal/mol, whereas -7.793 kcal/mol was the docking score of Roflumilast. Of the compounds screened, Gallotannins had the best docking score of −12.914 kcal/mol, followed by Rutin (−12.430 kcal/mol), β-glucans (−11.830 kcal/mol), Galactomannans (−11.680 kcal/mol), and Tribuloside (−10.957 kcal/mol), which were found to exhibit excellent geometric complementarity in the catalytic cavity of PDE4. Additionally, the EVDW values of Glide indicated good hydrophobicity of the binding of these phytoconstituents and their steric fit into the receptor binding pocket.

Molecular docking alone does not mean to be a good indicator of the thermodynamic stability of the protein-ligand complex, although Gallotannins had the highest docking score. Thus, the docked complexes were further analysed by Prime binding free energy (MM-GBSA). Interestingly, Ellagic acid showed the most favourable binding free energy (ΔGbind = −72.56 kcal/mol) and was able to bind better than all the other compounds screened and the reference inhibitor Roflumilast (ΔGbind = −49.18 kcal/mol). The rest of the phytoconstituents had the ΔGbind values in the range of −68.80 to −46.35 kcal/mol, with Tribuloside (−68.80 kcal/mol), Gallotannins (−68.34 kcal/mol), Polygonatoside A (−65.54 kcal/mol), and Rutin (−62.60 kcal/mol) having relatively stable ΔGbind values. Although Ellagic acid had a comparatively moderate docking score, the binding free energy was found to be substantially lower, suggesting that the protein-ligand interaction is energetically more stable; between the two, MM-GBSA analysis is more important to prioritise leads with docking analysis.

Energy decomposition analysis also gave insightful information about the intermolecular forces in the catalytic pocket in determining ligand recognition. Rutin showed the highest value of electrostatic contribution (ΔCoul = −74.70 kcal/mol), followed by Galactomannans (−72.67 kcal/mol) and β-glucans (−73.24 kcal/mol), showing that the electrostatic interaction is important towards the stabilization of these highly hydroxylated phytoconstituents. In contrast, Ellagic acid strongly interacted with a favorable Coulombic energy (ΔCoul = −29.62 kcal/mol), but an overall stable binding free energy, indicative of a combined effect of hydrogen bonding, π–π stacking, van der Waals interactions and hydrophobic contacts, rather than electrostatic interactions only. Of the ligands studied, Galactomannans (ΔHbond = −5.99 kcal/mol) and β-glucans (ΔHbond = −5.89 kcal/mol), which possessed the largest contribution

of hydrogen-bonding interactions, had the strongest hydrogen-bond energy, while Ellagic acid possessed a comparatively moderate hydrogen-bond energy (ΔHbond = −0.93 kcal/mol) and other non-covalent interactions played a significant role in the overall stability of binding. While all the phytoconstituents showed excellent docking scores, Ellagic acid was chosen as the lead compound due to its consistently most favorable thermodynamic binding free energy with a stable interaction profile with the catalytic pocket of PDE4. This remark highlights the importance of using MM-GBS calculations to obtain a more realistic estimation of the stability of ligand binding than using docking scores alone. Thus, Ellagic acid was chosen for further molecular dynamics simulation and in vitro biological validation for in-depth investigation of its therapeutic potential against COPD.

Residue-wise interaction analysis of the above complex revealed that Ellagic acid is very well accommodated in the catalytic pocket of PDE4, and in the binding conformation it is stabilized by hydrogen bonding, aromatic π–π stacking and hydrophobic interaction (Fig. 4A and 4B). A typical hydrogen bond was observed between the ligand and TYR159 that is crucial for the stabilization of the polyphenolic scaffold in the binding cavity. Moreover, the fused aromatic ring system of Ellagic acid also had π–π stacking interactions with PHE372 and TYR159, which also contributed to the stability of the protein–ligand complex. The ligand was surrounded by several hydrophobic amino acid residues, which provided favorable van der Waals and hydrophobic interactions that favored the accommodation of the ligand in the catalytic site, such as MET273, MET357, ILE336, ILE376, LEU319 and PHE340. Additionally, the binding pocket was also closed by polar residues GLN369, SER368, ASN321 and HIS164 and the catalytic residue ASP318 and the positively charged HIP160 were found near the ligand, which provided an electrostatically favorable environment for ligand complex formation. Multiple hydroxyl and lactone groups of Ellagic acid allowed favourable interaction with the active-site residues while the rigid fused dibenzopyranone framework allowed stable aromatic interaction within the hydrophobic cavity (Fig. No. 1). All these secondary non-covalent interactions synergistically contributed to a compact and energetically favorable binding orientation and the better MM-GBSA binding free energy obtained for Ellagic acid as compared to the reference inhibitor Roflumilast, suggesting its potential as a better natural inhibitor of PDE4 enzyme.

Table No. 1 Comparative molecular docking scores and MM-GBSA binding free energy values of the prioritized phytoconstituents screened against the catalytic domain of phosphodiesterase-4 (PDB ID: 4WCU)

S. No.	Compound Code	Glide Gscore	Glide evdw	XP Gscore	MM-GBSA ΔG Bind	MM-GBSA ΔHbond	MM-GBSA ΔCoul
1.	Ellagic acid	-9.262	-33.666	-9.262	-72.56	-0.93	-29.62
2.	Tribuloside	-10.957	-50.618	-10.957	-68.80	-0.80	-62.13
3.	gallotannins	-12.914	-45.305	-12.914	-68.34	-2.78	-63.75
4.	Polygonatoside A	-9.223	-43.351	-9.223	-65.54	-4.39	-53.13
5.	Rutin	-12.430	-38.228	-12.430	-62.60	-2.24	-74.70
6.	beta-glucans	-11.830	-36.087	-11.830	-57.49	-5.89	-73.24
7.	Galactomannans	-11.680	-35.511	-11.680	-57.09	-5.99	-72.67
8.	Beta-D-glucans	-10.224	-36.552	-10.224	-55.72	-3.44	-64.00
9.	Isoquercitrin	-9.173	-38.569	-9.173	-50.18	-0.16	-42.74
10.	α-Tocopherol	-9.484	-41.190	-9.484	-46.35	0.68	-7.29
11.	Roflumilast	-7.793	-33.004	-7.793	-49.18	-0.89	-12.19

Table No. 2 Physicochemical and cheminformatics characteristics of the lead compound Ellagic acid

Sl. No	Parameter	Details
1.	Compound ID	5281855
2.	IUPAC Name	6,7,13,14-tetrahydroxy-2,9-dioxatetracyclo[6.6.2.04,16.011,15]hexadeca-1(15),4,6,8(16),11,13-hexaene-3,10-dione
3.	Molecular Formula	$C_{14}H_6O_8$
4.	Molecular Weight	302.19 g/mol
5.	Exact Mass	302.00626715 Da
6.	SMILES Notation	C1=C2C3=C(C(=C1O)O)OC(=O)C4=CC(=C(C(=C43)OC2=O)O)O
7.	InChIKey	AFSDNFLWKVMVRB-UHFFFAOYSA-N
8.	Compound Class	Phenols and Cresols

9.	Predicted Biological Relevance	Inhibition of xanthine oxidase assessed as conversion of xanthine to uric acid incubated
10.	Role in Present Study	Lead compound selected for docking, MM-GBSA, molecular dynamics, and in vitro biological evaluation

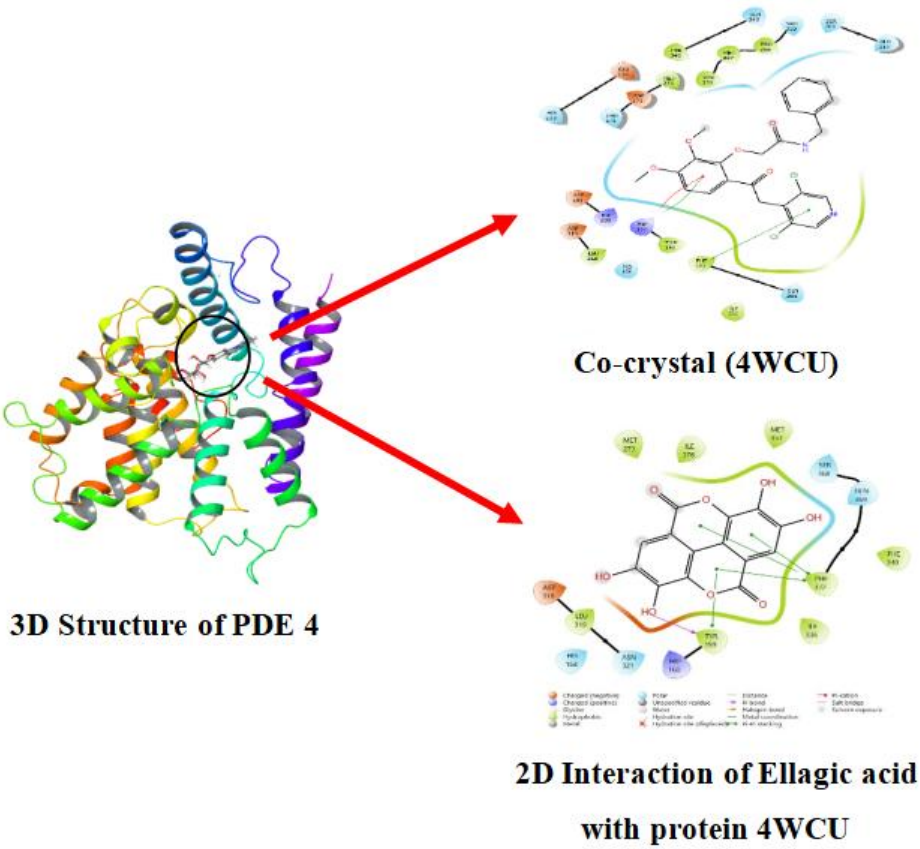

Fig. No. 1 Two-dimensional binding interaction profile of the computationally prioritized compound Ellagic acid and Co-crystal (4WCU) with the catalytic binding in PDE4 (PDB ID: 4WCU)

3.2 Toxicity Profile

The toxicity profile of prioritized phytoconstituents was predicted by using the web server of ProTox-3.0, and the information is presented in Table 3. The selected compounds had a wide range of predicted acute oral toxicities, ranging from LD_{50} of 51 mg/kg to 5000 mg/kg and toxicity classes ranged from 3–5. The compound with the lowest predicted LD_{50} is Ellagic acid with a toxicity class of 5, meaning that it is relatively not toxic when ingested orally. In the same manner, Rutin, Isoquercitrin, α-Tocopherol and Gallotannins also fall under toxicity class 5, which signifies that such phytoconstituents have favorable safety profiles as compared to the other phytoconstituents screened. Tribuloside and Cedeodarin, on the other hand, were classified as toxicity class 4, with the β-glucans, galactomannans, and Myricetin being classified as toxicity class 3, which indicate comparatively higher predicted acute toxicity.

Average similarity and prediction accuracy obtained by the ProTox-3.0 platform were used to check the reliability of the computational predictions. Some of the compounds obtained, such as Tribuloside, Myricetin, β-glucans and Rutin, had an average similarity of 100%, which means that there is a high similarity in structure to compounds found in the reference toxicity database. The prediction accuracy corresponding to each varied from 67.38% to 100%, which is an indication of the robustness of the computational toxicity assessment. Ellagic acid showed an average similarity of 53.49% and a prediction accuracy of 67.38%, which was similar to the reference drug Roflumilast (54.39% and 67.38%), respectively, suggesting good confidence in the predicted toxicity profile of ellagic acid.

In general, the computational toxicity assessment indicates that Ellagic acid has a favourable predicted safety profile with its high LD_{50} value (5000 mg/kg) and toxicity class 5, which means Ellagic acid has low acute oral toxicity as compared to some of the other prioritized phytoconstituents. While these in silico toxicity predictions can be helpful in early-stage lead optimization and compound prioritization, they can only be taken as preliminary and should be supported by a comprehensive in vitro and in vivo toxicological investigation before clinical translation.

Table No. 3 Predicted acute oral toxicity and safety profile of the prioritized phytoconstituents obtained using the ProTox-3.0 web server

Sl. No	Coconut ID	Predicted LD50	Predicted Toxicity Class	Average similarity	Prediction accuracy
1	Ellagic acid	5000mg/kg	5	53.49%	67.38%
2	Tribuloside	1190mg/kg	4	100%	100%
3	gallotannins	2260mg/kg	5	76.41%	69.26%
4	Myricetin	159mg/kg	3	100%	100%
5	Rutin	5000mg/kg	5	100%	100%
6	beta-glucans	51mg/kg	3	100%	100%
7	Galactomannans	51mg/kg	3	97.92%	72.9%
8	Cedeodarin	2000mg/kg	4	83.23%	70.97%
9	Isoquercitrin	5000mg/kg	5	95.7%	72.9%
10	α-Tocopherol	5000mg/kg	5	82.25%	70.97%
11	Roflumilast	2000mg/kg	4	54.39%	67.38%

3.3 Molecular Dynamics (MD) simulation

To further explore the dynamic stability of the ligand of interest, which was computationally prioritized in the catalytic pocket of PDE4, a 200 ns molecular dynamics (MD) simulation was conducted for both the PDE4–Ellagic acid and PDE4–Roflumast complexes. The stability of the complexes was initially assessed using the root mean square deviation (RMSD) of backbone atoms of the protein and the ligand from the trajectory of the simulation (Fig. No. 2A and 2B). The PDE4-Ellagic acid complex was seen to have an initial equilibration period for the first 20–30ns, after which the protein backbone starts to attain a stable structure, although moderate fluctuations are observed throughout the rest of the trajectory. The ligand made some conformational changes in the initial part of the trajectory but eventually evolved to a stable binding conformation in the catalytic cavity without breaking free from the binding pocket throughout the trajectory. The PDE4–Roflumilast complex, on the other hand, also reached equilibrium after the equilibration process, but there were relatively larger fluctuations in the trajectory, which indicates that the ligand was more flexible in the active site than the PDE4–Milrinone complex. In general, both complexes showed no structural changes throughout the 200ns simulation, with the PDE4–Ellagic acid complex showing a more consistent conformational behavior, suggesting a greater dynamic stability as compared to the reference inhibitor (Fig. No. 2).

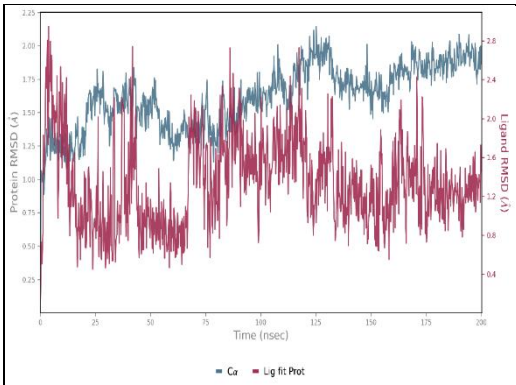

Fig. No. 2A Root mean square deviation (RMSD) trajectory of the PDE4–Ellagic acid complex over a 200 ns molecular dynamics simulation

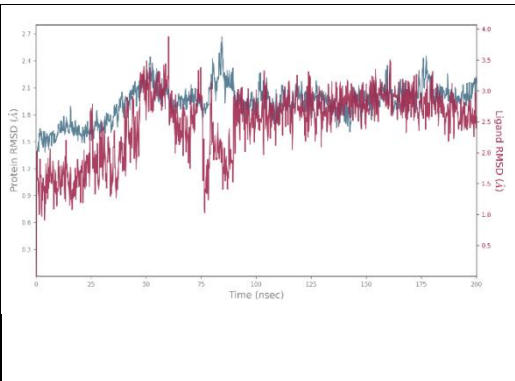

Fig. No. 2B Root mean square deviation (RMSD) trajectory of the PDE4–Roflumilast complex over a 200 ns molecular dynamics simulation

Fig. No. 2 Root mean square deviation (RMSD) profiles of the PDE4–Ellagic acid and PDE4–Roflumilast complexes during the 200 ns molecular dynamics simulation

RMSF profiles were then used for analysing the flexibility of each residue of the PDE4 protein in the presence of both ligands (Fig. No. 3). The fluctuation of most of the amino acid residues was low in both complexes, showing that there was no change in the protein architecture during the simulation. Not surprisingly, increased fluctuations were primarily localized to solvent-accessible loop regions of the structure, with residues forming the catalytic binding pocket of the

enzyme being relatively rigid. The PDE4–Ellagic acid complex revealed relatively smaller fluctuations for most of the catalytic site residues, and thus the ligand binding was able to restrict local protein mobility. The PDE4–Roflumilast complex, on the other hand, showed overall increased flexibility at a few loop regions, indicating less efficient stabilization of the receptor structure. Significantly, the important catalytic residues participating in the recognition of ligands were stable during the simulation, and this confirmed the stability of the protein–ligand interactions observed in molecular docking (Fig. No. 3).

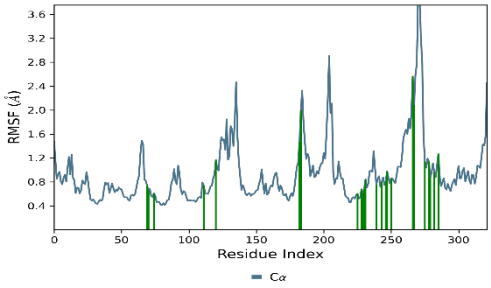

Fig. No. 3A Root Mean Square Fluctuation (RMSF) profile of amino acid residues of the PDE4–Ellagic acid complex during the 200 ns molecular dynamics simulation

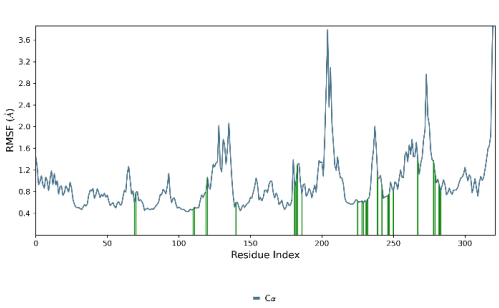

Fig. No. 3B Root Mean Square Fluctuation (RMSF) profile of amino acid residues of the PDE4–Roflumilast complex during the 200 ns molecular dynamics simulation

Fig. No. 3 Comparative root mean square fluctuation (RMSF) profiles of the PDE4–Ellagic acid and PDE4–Roflumilast complexes during the 200 ns molecular dynamics simulation

Protein–ligand interaction histogram analysis also revealed that the intermolecular interactions remained constant throughout the time of the simulations (Fig. No. 4). Ellagic acid was able to maintain frequent interaction with the key residues of the catalytic cavity of the enzyme, namely, TYR159, ASP318, PHE372, GLN369, ASN321 and HIS164, suggesting that it was present at the catalytic cavity for a prolonged time. The interaction profile showed that the hydrogen bonding was the dominant stabilizing force and the hydrophobic and water-mediated contacts were also found to help the ligand to retain its orientation during the trajectory. By contrast, Roflumilast showed fewer persistent contacts and predominantly interacted with ASP318, PHE372, GLN369, ILE336 and TYR159 with lower frequencies of contact for a number of adjacent residues. The general interaction network seen for Ellagic acid indicates better retention in the catalytic pocket and resistance to conformational changes during simulations.

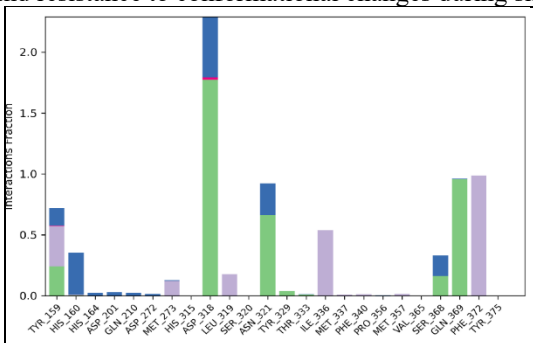

Fig. No. 4A Ligand atom interactions histograms of Ellagic acid with the residues of 4WCU.pdb

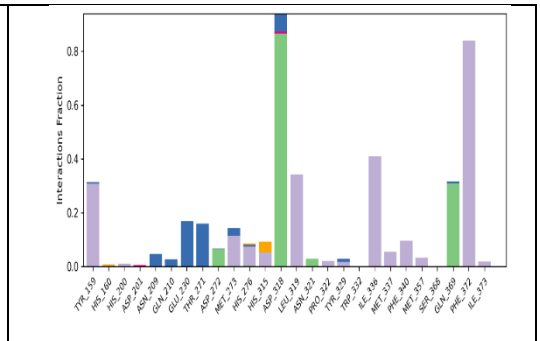

Fig. No. 4B Ligand atom interactions histograms of Roflumilast with the residues of 4WCU.pdb

Fig. No. 4 Comparative protein–ligand interaction histogram analysis of the PDE4–Ellagic acid and PDE4–Roflumilast complexes during the 200 ns molecular dynamics simulation

The representative 2D interaction diagram performed from the MD trajectory also verified the stability of Ellagic acid binding mode (Fig. No. 5). Ellagic acid maintained a consistent hydrogen bond network with the backbone of TYR159 and GLN369 throughout the simulation and some other interactions such as the backbone hydrogen bonding with ASP318, hydrogen bonding with the side chain of ASN321 and π–π stacking and hydrophobic interactions with HIS164 and PHE372 also helped in stabilization of the complex. Due to the multiple hydroxyl and lactone functionalities of Ellagic acid, multiple complementary interactions were formed at the catalytic cavity, which resulted in less replacement of the ligands in the simulation. The Roflumilast complex, on the other hand, has fewer simultaneous interactions, and the majority of the contacts are with ASP318, PHE372, and surrounding hydrophobic residues. The multiple contacts of

Ellagic acid with the PDE4 active site in the form of a multivalent interaction network might explain the better thermodynamic stability, predicted by MM-GBSA analysis, and the good dynamic behavior during the 200ns simulation.

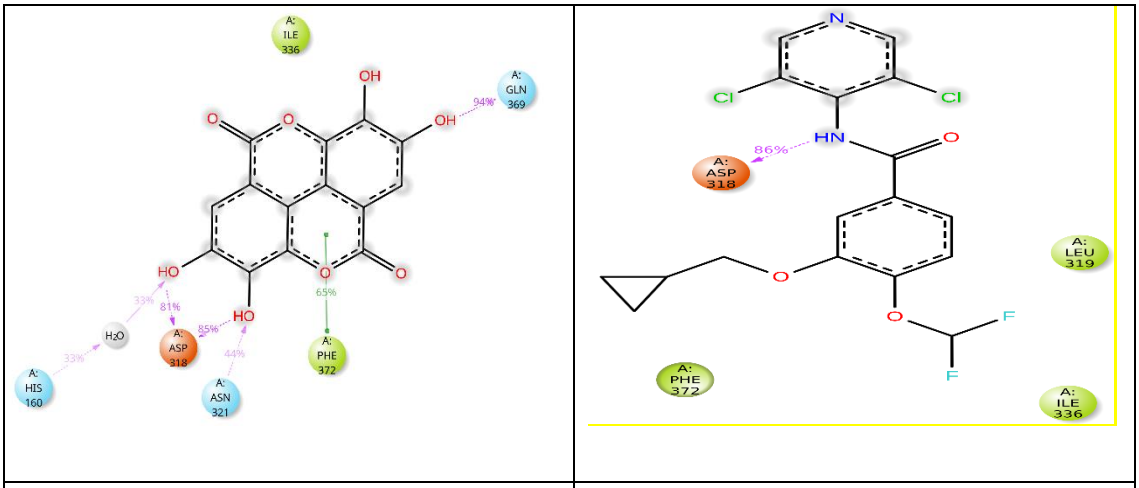

Fig. No. 5A Ligand atom 2D interactions of Ellagic acid with residues of 4WCU.pdb	Fig. No. 5B Ligand atom 2D interactions of Roflumilast with residues of 4WCU.pdb

Fig. No. 5 Protein–ligand 2D interaction analysis during molecular dynamics simulation of PDE4–Ellagic acid and PDE4–Roflumilast complex

Overall, the 200 ns molecular dynamics simulation indicated that the PDE4–Ellagic acid complex maintained structural stability during the entire simulation and always retained important interactions with the catalytic binding pocket. Overall RMSD, RMSF, protein–ligand interaction, and two-dimensional interaction analysis results reveal that Ellagic acid strongly interacts with PDE4 to form a stable complex at a dynamically stable state as compared to the reference inhibitor Roflumilast. These results further validate the molecular docking and MM-GBSA results and also suggest that Ellagic acid could be a potential natural lead compound to develop PDE4-targeted therapeutics for chronic obstructive pulmonary disease.

3.4 In vitro Study

3.4.1 Antioxidant Assay

Ellagic acid was tested for antioxidant activity at various concentrations (0-500µg/mL) by DPPH free radical scavenging assay. DPPH radicals have a distinctive deep purple colour which will fade after they have been reduced by a hydrogen- or electron-donating antioxidant molecule to a yellowish colour, causing a decrease in absorbance at 517 nm. As shown in Table No. 4 and Fig. No. 6, the free radical scavenging activity of No.11 Ellagic acid increased as the concentration increased. The untreated control did not show any inhibition, while the inhibition was 36.66 ± 0.14% at 10 µg/mL. The radical scavenging activity progressively increased to 46.12 ± 0.16%, 56.62 ± 0.17%, 67.32 ± 0.08%, 73.06 ± 0.11%, and 75.34 ± 0.10% at concentrations of 25, 50, 75, 100, and 125 µg/mL, respectively. Under higher concentrations (250 and 500 µg/mL), Ellagic acid showed a maximum scavenging activity of 86.11 ± 0.23% and 86.56 ± 0.09%, respectively, which means that the antioxidant effect of Ellagic acid was almost saturated. The IC50 (concentration to inhibit 50% of DPPH radicals) was found to be about 38 µg/mL, which showed potent free radical scavenging ability of Ellagic acid. These results support the potent antioxidant activity of Ellagic acid that could play a role in its protective effect against oxidative stress in COPD.

Table No. 4 Antioxidant activity of Ellagic acid in different concentrations

Sl. No	Conc. in µg/mL	% Inhibition
1.	0	0.00
2.	10	36.66 ± 0.14
3.	25	46.12 ± 0.16
4.	50	56.62 ± 0.17
5.	75	67.32 ± 0.08
6.	100	73.06 ± 0.11
7.	125	75.34 ± 0.10
8.	250	86.11 ± 0.23
9.	500	86.56 ± 0.09

Values are mean ± S.E.M, n=3 symbols represent statistical significance

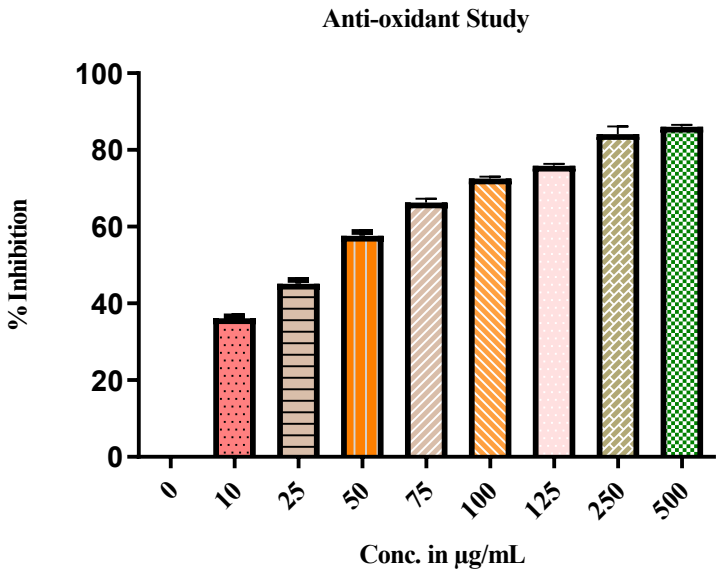

Fig. No. 6 Concentration-dependent DPPH radical scavenging activity of Ellagic acid under in vitro conditions. The antioxidant activity increased progressively with increasing concentrations of Ellagic acid, with the highest concentration (green bar) exhibiting significantly greater radical scavenging activity than the lowest concentration (orange bar), indicating enhanced antioxidant potential

3.4.2 Cell Viability Assay

Sulforhodamine B (SRB) Assay was used to assess the cytotoxicity of Ellagic acid on normal human bronchial epithelial (BEAS-2B) cells. As revealed in Table No. 5 and Fig. No. 7, Ellagic acid showed a concentration-dependent decrease in cell viability. In the case of 10 µg/mL, it can be seen that 76.27 ± 0.06% of cells remained viable, which means that all the experimental conditions were acceptable for cellular tolerance. The cell viability was further decreased to 65.39 ± 0.04% by the 100 µg/mL concentration and 42.84 ± 0.20% by the 1000 µg/mL concentration, indicating a higher level of cytotoxicity at higher concentrations. The untreated control had 100% cell viability for the duration of the experiment. These results suggest that Ellagic acid has a relatively low level of cytotoxicity at low concentrations and concentration-dependent growth inhibition at higher concentrations. The cell viability assay was used to provide the preliminary cellular safety profile of Ellagic acid and is not necessarily a direct readout of PDE4 inhibitory activity or therapeutic activity.

Table No. 5 Cell viability % of Ellagic acid against BEAS2B cell line

Sl. No.	Concentration (µg/ml)	Cell viability (%)
1.	10	76.27 ± 0.06
2.	100	65.39 ± 0.04
3.	1000	42.84 ± 0.2
4.	Normal Control	100 ± 0.00

Values are mean ± S.E.M, n=3 symbols represent statistical significance

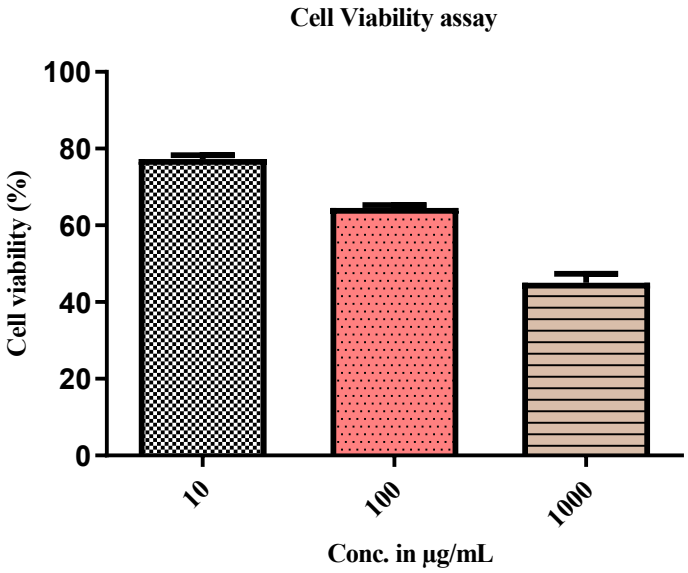

Fig. No. 7 Concentration-dependent BEAS-2B cell viability following treatment with Ellagic acid, as determined by the SRB assay. Cell viability remained high at lower concentrations and gradually declined with increasing drug concentration, demonstrating relatively low cytotoxicity toward normal bronchial epithelial cells under the experimental conditions

3.4.3 SRB Assay (IC50)

To further compare the cytotoxic effects of Ellagic acid and reference PDE4 inhibitor, Roflumilast on BEAS-2B cells, their respective IC_{50} values were also calculated from the SRB assay. As shown in Table No. 6, Ellagic acid resulted in an IC_{50} value of 735.4 ± 0.04 µg/mL, which was relatively high when compared to Roflumilast, which had a significantly lower IC_{50} value of 4.3 ± 0.07 µg/mL. There is a significant difference between the IC_{50} of Ellagic acid and the reference drug in the same experimental condition, which suggests lower toxicity and enhanced cellular tolerability of Ellagic acid than the reference drug towards normal bronchial epithelial cells. The results suggest that Ellagic acid has a relatively good in vitro safety profile since BEAS-2B cells are normal lung epithelial cells. However, these observations should be considered in the context of the cell-based cytotoxicity assessment only and not directly define comparative anti-inflammatory activity, PDE4 inhibitory potency or clinical safety.

Table No. 6 IC50 value of Ellagic acid and Roflumilast against BEAS2B

Sl. No.	Compounds	IC_{50} Value (µg/ml)
1.	Ellagic acid	735.4 ± 0.04
2.	Roflumilast	4.3 ± 0.07

3.4.4 Pro-inflammatory cytokines assay

The anti-inflammatory effect of Ellagic acid was assessed by determining the level of pro-inflammatory cytokines secreted by LPS-stimulated RAW264.7 macrophages. As shown in Fig No. 8, 9 and 10, LPS-induced secretion of TNF-α, IL-6 and IL-1β was significantly decreased after treatment with Ellagic acid as compared to the inflammatory control group. The inhibitory effect was found to be concentration-dependent, with higher concentrations of the treatment resulting in suppression of the production of cytokines. The highest concentration of Ellagic acid had the biggest effect in reducing the release of the cytokines, demonstrating that the LPS-induced inflammatory response was effectively reduced. The decreased production of these cytokines may contribute to the anti-inflammatory property of Ellagic acid, as overproduction of these cytokines is involved in the chronic inflammation of the airways in COPD. These findings, however, are the biological responses under current experimental conditions, and shouldn't necessarily be translated into direct evidence of selective PDE4 inhibition, as additional mechanistic validation is required.

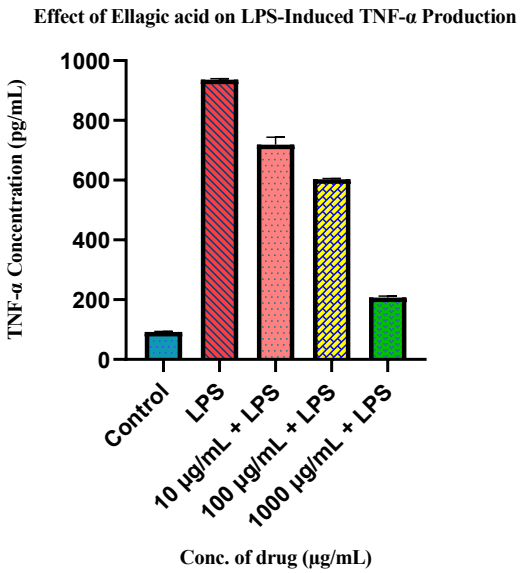

Fig. No. 8 Effect of Ellagic acid on LPS-induced TNF-α production in RAW264.7 macrophages. The LPS-treated inflammatory control group (red bar) exhibited markedly elevated TNF-α levels, whereas treatment with Ellagic acid (yellow, light green, and green bars) produced a concentration-dependent reduction in TNF-α production, indicating significant anti-inflammatory activity

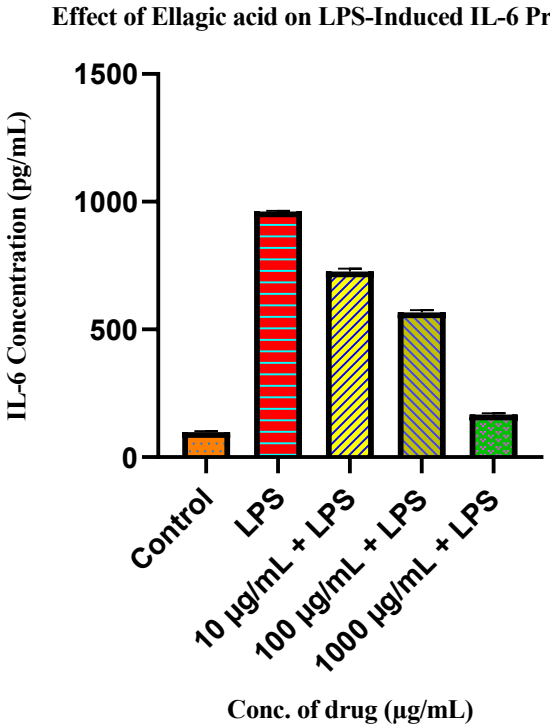

Fig. No. 9 Effect of Ellagic acid on IL-6 production in LPS-stimulated RAW264.7 macrophages. The LPS-treated inflammatory control group (red bar) exhibited markedly elevated IL-6 levels, whereas treatment with increasing concentrations of Ellagic acid (yellow, light green, and green bars) significantly and concentration-dependently reduced IL-6 production, indicating potent anti-inflammatory activity under the experimental conditions

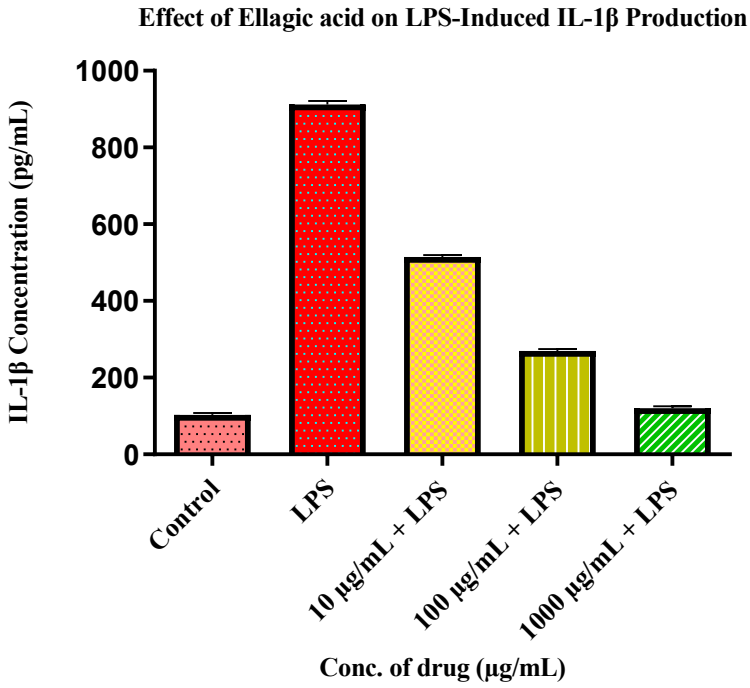

Fig. No. 10 Effect of Ellagic acid on IL-1β production in LPS-stimulated RAW264.7 macrophages. The LPS-treated inflammatory control group (red bar) exhibited markedly elevated IL-1β levels, whereas treatment with increasing concentrations of Ellagic acid (yellow, light green, and green bars) significantly and concentration-dependently reduced IL-1β production, indicating potent anti-inflammatory activity under the experimental conditions

3.4.5 Nitric oxide inhibition assay

The production of nitric oxide (NO) production in macrophages stimulated with LPS by the effect of Ellagic acid was studied. The production of NO was significantly elevated in the LPS (1 µg/mL) treated group as compared with the normal control, reflecting successful induction of inflammatory response. Fig. No. 10 shows that the amounts of nitric oxide released in response to Ellagic acid treatment at 10, 100 and 1000 µg/mL were significantly lower than the LPS treated group. The inhibitory effect was concentration-dependent and at the highest concentration the nitric oxide production was most suppressed. These data suggest that Ellagic acid is able to inhibit nitric oxide production in response to LPS, and therefore may be able to regulate inflammatory mediators production under the experimental conditions used.

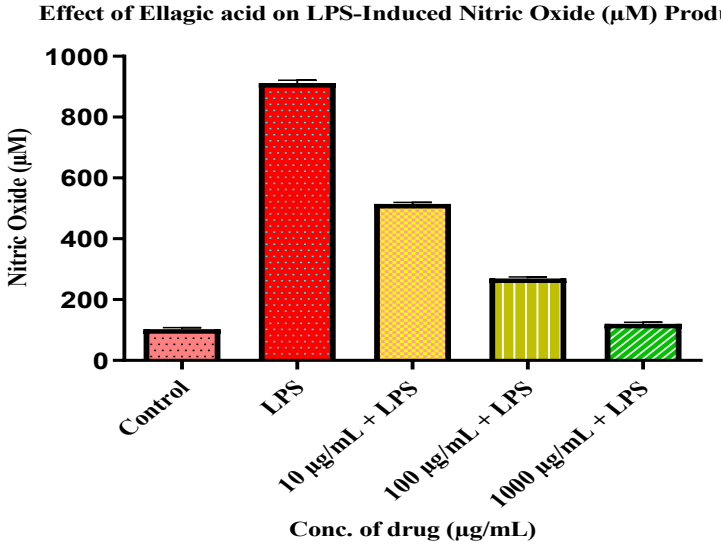

Fig. No. 11 Effect of Ellagic acid on nitric oxide (NO) production in LPS-stimulated RAW264.7 macrophages. The LPS-treated inflammatory control (red bar) exhibited the highest NO production, whereas treatment with increasing concentrations of Ellagic acid (yellow, light green, and green bars) significantly and concentration-

dependently suppressed NO production. The untreated normal control (orange bar) showed basal NO levels, demonstrating the anti-inflammatory potential of Ellagic acid under the experimental conditions

3.4.6 cAMP Level Measurement

The functional effects of Ellagic acid on intracellular cAMP signalling were tested in BEAS-2B cells stimulated with LPS (10 µg/mL) and treated with Ellagic acid to set up an in vitro COPD inflammatory model. As shown in Table No. 7 and Fig. No. 11, the mean value of the first harmonic THD at 40% load is 1.9452%. The untreated control group (No.15) had an intracellular cAMP level of 27.5 ± 0.1 pmol/mg protein. The intracellular cAMP level was significantly decreased in the LPS-stimulated group (11.47 ± 0.06 pmol/mg protein), and the inflammatory model was successfully induced. Partial recovery of the impaired cAMP signalling pathway was observed by the treatment with Ellagic acid (10 µM) which showed significant recovery of the intracellular level of cAMP to 18.36 ± 0.03 pmol/mg protein. The treatment concentration was increased to 100 µM for a further increase in the levels of intracellular cAMP to 23.74 ± 0.50 pmol/mg protein, which was near the untreated control. These results suggest that Ellagic acid is able to reverse the cAMP depletion by LPS, as observed by the concentration-dependent restoration of the intracellular cAMP levels. The increase in cAMP levels is consistent with the suggested mechanism of PDE4 inhibition by the computational studies, since PDE4 was found to be the main enzyme that breaks down cAMP in inflammatory cells from the airways. Taken together, the data presented here indicate that Ellagic acid recovers the intracellular cAMP signalling under inflammatory conditions and could thus be a valuable natural therapeutic compound for COPD via modulation of the cAMP/PDE4 pathway.

Table No. 7 Quantification of Intracellular cAMP Levels in BEAS2B Cells following Treatment with Ellagic acid

Sl. No.	Experimental Group	Intracellular cAMP Level (pmol/mg protein)
1.	Control Group	27.5 ± 0.1
2.	LPS (10 µg/mL)	11.47 ± 0.06
3.	LPS + Drug (10 µM)	18.36 ± 0.03
4.	LPS + Drug (100 µM)	23.74 ± 0.5

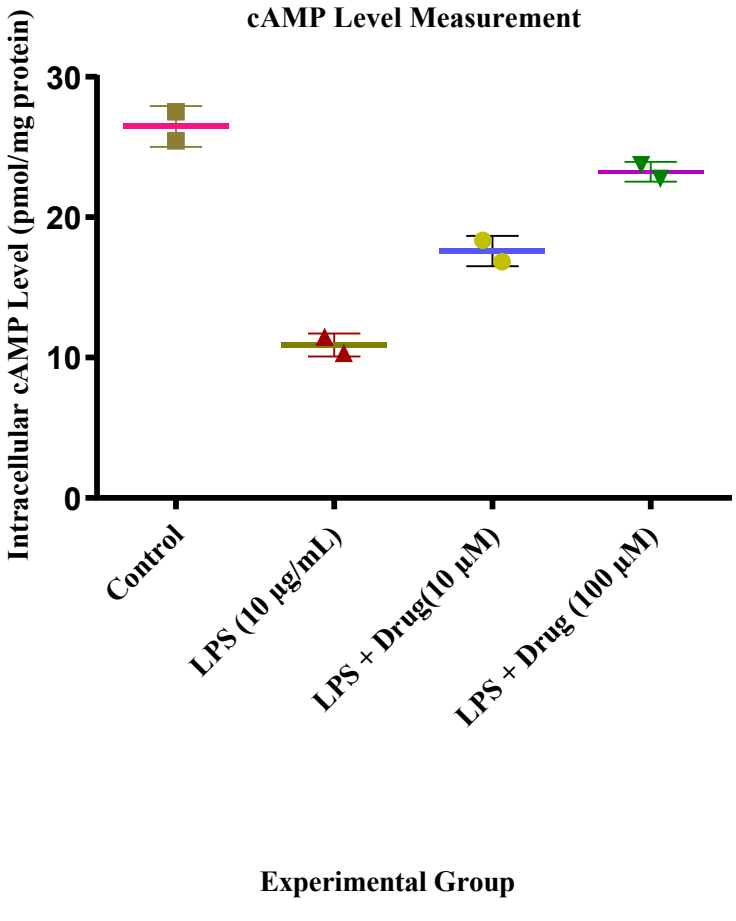

Fig. No. 12 Effect of Ellagic acid on LPS-induced cAMP level measurement in RAW264.7 macrophage cells at various concentrations of Ellagic acid. Treatment with Ellagic acid resulted in a concentration-dependent increase in the level of cAMP in comparison to LPS-treated controls, suggesting a PDE4 Inhibitor

Conclusion

In the present study, an integrated computational and experimental approach was successfully utilized to investigate Ellagic acid as a potential natural phosphodiesterase-4 (PDE4) inhibitor for the management of chronic obstructive pulmonary disease (COPD). Through systematic virtual screening, Ellagic acid was identified as one of the most promising candidates for further investigation, as part of a virtual screening workflow of Ayurvedic phytoconstituents. Molecular docking showed that Ellagic acid fits well in the PDE4 catalytic pocket (PDB ID: 4WCU) with hydrogen bonding, π-π stacking and hydrophobic interactions with important catalytic residues such as TYR159, GLN369, PHE372, ASP318, and HIS160. The subsequent MM-GBSA calculations showed that the protein-ligand complex was stable with a favorable binding free energy; the molecular dynamics simulation showed that the structure of the complex remained stable throughout the 200 ns simulation with low RMSD, limited fluctuations of residues and persistent protein-ligand interactions. Combined with the computational results, the overall data suggest that Ellagic acid might have a stable binding mode that could be able to fit the catalytic pocket of PDE4.

Additionally, in silico pharmacokinetic screening revealed that Ellagic acid has the desirable drug-like properties with a favourable predicted toxicity profile, making it suitable for further pharmaceutical development. This was supported by experimental validation, which showed that Ellagic acid possesses strong antioxidant activity, low toxicity toward normal BEAS-2B bronchial epithelial cells, a strong inhibitory effect on the production of pro-inflammatory mediators (TNF-α, IL-6, IL-1β and nitric oxide) in LPS-stimulated RAW264.7 macrophages, and the ability to restore intracellular cAMP levels in inflamed BEAS-2B cells. The biological results show that Ellagic acid was able to reduce oxidative stress and inflammatory response in COPD as well as modulate the functional activity of the cAMP signalling pathway, supporting the proposed mechanism of action of PDE4 inhibitors.

Overall, the use of molecular modelling, molecular dynamics simulations, ADMET prediction and in vitro biological evaluation strongly suggest that Ellagic acid is a good natural lead molecule for PDE4-targeted therapy for COPD. While the current results provide a comprehensive preclinical platform, further biochemical PDE4 enzyme inhibition studies, target validation, biochemical and in vivo efficacy/pharmacokinetic investigations are needed to verify the mechanism of action and therapeutic value before clinical translation. The present work is useful for future development of safe and natural PDE4 inhibitors as a treatment for chronic inflammatory airway diseases.

References

1. Delhaye S, Bardoni B. Role of phosphodiesterases in the pathophysiology of neurodevelopmental disorders. Mol Psychiatry 2021;26:4570–82. https://doi.org/10.1038/s41380-020-00997-9.
2. Nourian YH, Salimian J, Ahmadi A, et al. cAMP-PDE signaling in COPD: Review of cellular, molecular and clinical features. Biochemistry and Biophysics Reports 2023;34:101438. https://doi.org/10.1016/j.bbrep.2023.101438.
3. Lugnier C. The Complexity and Multiplicity of the Specific cAMP Phosphodiesterase Family: PDE4, Open New Adapted Therapeutic Approaches. International Journal of Molecular Sciences 2022;23:10616. https://doi.org/10.3390/ijms231810616.
4. Zhao P, Chen S-K, Cai Y-H, et al. The molecular basis for the inhibition of phosphodiesterase-4D by three natural resveratrol analogs. Isolation, molecular docking, molecular dynamics simulations, binding free energy, and bioassay. Biochimica et Biophysica Acta (BBA) - Proteins and Proteomics 2013;1834:2089–96. https://doi.org/10.1016/j.bbapap.2013.07.004.
5. Huang H. Natural PDE4 inhibitors from plants: A comprehensive review of discovery, structure-activity relationships, and clinical translation potential. European Journal of Medicinal Chemistry 2026;315:118960. https://doi.org/10.1016/j.ejmech.2026.118960.
6. Vaghela AR. Molecular docking in drug design: Basic concepts and application spectrums. Am J Pharmacother Pharm Sci 2026;5. https://doi.org/10.25259/AJPPS_2026_001.
7. Subramaniam T, Mualif SA, Chan WH, et al. Unlocking the potential of in silico approach in designing antibodies against SARS-CoV-2. Front Bioinform 2025;5:1533983. https://doi.org/10.3389/fbinf.2025.1533983.
8. Wang W, Wang S, Liu Y, et al. Ellagic Acid: A Dietary-Derived Phenolic Compound for Drug Discovery in Mild Cognitive Impairment. Front Aging Neurosci 2022;14:925855. https://doi.org/10.3389/fnagi.2022.925855.
9. Ganjali S, Matbou Riahi M, Mahboobnia K, et al. An in vitro investigation of the effects of urolithins A and B on low-density lipoprotein uptake and its regulatory genes. Arch Med Sci 2023;19:1832–41. https://doi.org/10.5114/aoms/168120.
10. Oliveira FL de, Arruda TYP, Lima R da S, et al. Pomegranate as a natural source of phenolic antioxidants: a review. Journal of Food Bioactives 2020;9:10–22. https://doi.org/10.31665/JFB.2020.9214.
11. Wang L, Fischmeister R, Manoury B. Cyclic Nucleotide Phosphodiesterase Families as Targets to Treat Pulmonary Arterial Hypertension: Beyond PDE5 Inhibitors? Cells 2025;14:1670. https://doi.org/10.3390/cells14211670.
12. Fan T, Wang W, Wang Y, et al. PDE4 inhibitors: potential protective effects in inflammation and vascular diseases. Front Pharmacol

2024;15:1407871. https://doi.org/10.3389/fphar.2024.1407871.
13. Peng T, Qi B, He J, et al. Advances in the Development of Phosphodiesterase-4 Inhibitors n.d.
14. Azam F, Khan MA, Khan A, et al. In silico and in vitro studies on the inhibition of laccase activity by Ellagic acid: Implications in drug designing for the treatment of Cryptococcal infections. Int J Biol Macromol 2022;209:642–54. https://doi.org/10.1016/j.ijbiomac.2022.04.060.
15. Alanzi AR, Alsalhi MS, Mothana RA, et al. Insilico discovery of novel Phosphodiesterase 4 (PDE4) inhibitors for the treatment of psoriasis: Insights from computer aided drug design approaches. PLoS One 2024;19:e0305934. https://doi.org/10.1371/journal.pone.0305934.
16. Kullappan M, Benedict BA, Rajajagadeesan A, et al. Ellagic Acid as a Potential Inhibitor against the Nonstructural Protein NS3 Helicase of Zika Virus: A Molecular Modelling Study. Biomed Res Int 2022;2022:2044577. https://doi.org/10.1155/2022/2044577.
17. Le VTT, Hung HV, Ha NX, et al. Natural Phosphodiesterase-4 Inhibitors with Potential Anti-Inflammatory Activities from Millettia dielsiana. Molecules 2023;28:7253. https://doi.org/10.3390/molecules28217253.
18. De Vita S, Lauro G, Ruggiero D, et al. Protein Preparation Automatic Protocol for High-Throughput Inverse Virtual Screening: Accelerating the Target Identification by Computational Methods n.d.
19. Binkowski TA, Jiang W, Roux B, et al. Virtual High-Throughput Ligand Screening. Methods Mol Biol 2014;1140:251–61. https://doi.org/10.1007/978-1-4939-0354-2_19.
20. Onisuru O, Achilonu I. High-throughput virtual screening and empirical validation of probable inhibitors of Plasmodium falciparum and vivax glutathione transferase using bromosulfophthalein as the benchmark ligand. International Journal of Biological Macromolecules 2025;302:140526. https://doi.org/10.1016/j.ijbiomac.2025.140526.
21. Huang Y, Benni S, Yadav UP, et al. Deploying the high-throughput virtual screening (HTVS) approach for the identification of new lactate dehydrogenase (LDH) inhibitors with anticancer assets. Sci Rep 2026;16:5921. https://doi.org/10.1038/s41598-026-36385-6.
22. Shen T, Shen H, Kong Y, et al. Structure-based virtual screening identifies novel small-molecule inhibitors targeting the endonuclease active site of APE1. Sci Rep 2026;16:21299. https://doi.org/10.1038/s41598-026-51975-0.
23. Zaman SR, Parvin MstS, Akter M, et al. Computational identification of natural inhibitors of human neutrophil elastase as potential therapeutics for chronic obstructive pulmonary disease. Immunobiology 2026;231:153209. https://doi.org/10.1016/j.imbio.2026.153209.
24. Menye C, Tjegbe MJM, Nkem C, et al. In silico identification of potential COX-2 inhibitors from sapelenins: molecular docking, molecular dynamics, MM-GBSA, DFT, and pharmacokinetic analysis. In Silico Research in Biomedicine 2026;2:100445. https://doi.org/10.1016/j.insi.2026.100445.
25. Johnston RC, Yao K, Kaplan Z, et al. Epik: pKa and Protonation State Prediction through Machine Learning n.d.
26. Han X, Guo K. Pharmacophore-based virtual screening of commercial databases against β-secretase 1 for drug development against Alzheimer's disease. Front Chem 2024;12:1412349. https://doi.org/10.3389/fchem.2024.1412349.
27. Mohamed FJ, Kuriakose BB, Alhazmi AH, et al. E-Pharmacophore and virtual screening reveal Apium graveolens as a therapeutic prospect for vitiligo. Results in Chemistry 2025;17:102610. https://doi.org/10.1016/j.rechem.2025.102610.
28. Alanzi AR, Alsalhi MS, Mothana RA, et al. Insilico discovery of novel Phosphodiesterase 4 (PDE4) inhibitors for the treatment of psoriasis: Insights from computer aided drug design approaches. PLoS One 2024;19:e0305934. https://doi.org/10.1371/journal.pone.0305934.
29. Pavan M, Menin S, Bassani D, et al. Qualitative Estimation of Protein–Ligand Complex Stability through Thermal Titration Molecular Dynamics Simulations. J Chem Inf Model 2022;62:5715–28. https://doi.org/10.1021/acs.jcim.2c00995.
30. Ahmad K, Ahmad SS, Choi I. Integrated virtual screening, ADMET profiling, and molecular dynamics simulations of novel natural HDAC6 inhibitors with the potential to ameliorate skeletal muscle degeneration. Sci Rep 2026;16:7840. https://doi.org/10.1038/s41598-026-39066-6.
31. Ribone SR. In Silico Methodology for Human Carboxylesterases 1 and 2 Isoforms Substrate Selectivity Study. In: Labrou N, editor. Targeting Enzymes for Pharmaceutical Development: Methods and Protocols, New York, NY: Springer US; 2026, p. 369–96. https://doi.org/10.1007/978-1-0716-5190-2_19.
32. Neelima N, Elrewey H, Smarakan S, et al. Machine learning-driven computational drug repurposing to identify new tubulin inhibitors against cancer. Bioorganic & Medicinal Chemistry 2026;136:118587. https://doi.org/10.1016/j.bmc.2026.118587.
33. Sabantsev MO, Brovin AN, Gureev MA, et al. Application of Rational Design and Molecular Metadynamics for the Estimation of Changes in Trans-Splicing Efficiency during the Mutagenesis of Ssp DnaE Intein. ACS Bio Med Chem Au n.d.;5:738–52. https://doi.org/10.1021/acsbiomedchemau.5c00091.
34. Jeeru TR, Palathoti N, Swaminathan G. Deciphering the Neuroprotective Potential of Piperine Derivatives: A Computational Study. ChemistrySelect 2026;11:e07487. https://doi.org/10.1002/slct.202507487.
35. Ogun OJ, Thaller G, Becker D. Molecular Structural Analysis of Porcine CMAH–Native Ligand Complex and High Throughput Virtual Screening to Identify Novel Inhibitors. Pathogens 2023;12:684. https://doi.org/10.3390/pathogens12050684.

36. Li C, Xu Y, Su W, et al. Structural insights into ligand recognition, selectivity, and activation of bombesin receptor subtype-3. Cell Reports 2024;43:114511. https://doi.org/10.1016/j.celrep.2024.114511.
37. Sahayarayan JJ, Rajan KS, Vidhyavathi R, et al. In-silico protein-ligand docking studies against the estrogen protein of breast cancer using pharmacophore based virtual screening approaches. Saudi J Biol Sci 2021;28:400–7. https://doi.org/10.1016/j.sjbs.2020.10.023.
38. kumar BH, Manandhar S, Mehta CH, et al. Structure-based docking, pharmacokinetic evaluation, and molecular dynamics-guided evaluation of traditional formulation against SARS-CoV-2 spike protein receptor bind domain and ACE2 receptor complex. Chem Zvesti 2022;76:1063–83. https://doi.org/10.1007/s11696-021-01917-z.
39. Najafi N, Fatemi MH. Computational design of PARP-1 inhibitors: QSAR, molecular docking, virtual screening, ADMET, and molecular dynamics simulations for targeted drug development. SAR and QSAR in Environmental Research 2025;36:205–46. https://doi.org/10.1080/1062936X.2025.2480859.
40. Le VTT, Hung HV, Ha NX, et al. Natural Phosphodiesterase-4 Inhibitors with Potential Anti-Inflammatory Activities from Millettia dielsiana. Molecules 2023;28:7253. https://doi.org/10.3390/molecules28217253.
41. Mohamed GA, Abdallah HM, Sindi IA, et al. Unveiling the potential of phytochemicals to inhibit nuclear receptor binding SET domain protein 2 for cancer: Pharmacophore screening, molecular docking, ADME properties, and molecular dynamics simulation investigations. PLoS One 2024;19:e0308913. https://doi.org/10.1371/journal.pone.0308913.
42. Bas DC, Rogers DM, Jensen JH. Very fast prediction and rationalization of pKa values for protein–ligand complexes. Proteins: Structure, Function, and Bioinformatics 2008;73:765–83. https://doi.org/10.1002/prot.22102.
43. Ibisanmi TA, Jiang X, Khan RA, et al. Multimodal computational discovery of MvfR inhibitors targeting quorum sensing in multi-drug-resistant Pseudomonas aeruginosa. Sci Rep 2026;16:20658. https://doi.org/10.1038/s41598-026-50613-z.
44. Rawat R, Verma SM. High-throughput virtual screening approach involving pharmacophore mapping, ADME filtering, molecular docking and MM-GBSA to identify new dual target inhibitors of PfDHODH and PfCytbc1 complex to combat drug resistant malaria. Journal of Biomolecular Structure and Dynamics 2021;39:5148–59. https://doi.org/10.1080/07391102.2020.1784288.
45. Jin J, Mazzacuva F, Crocetti L, et al. PDE4 Inhibitors: Profiling Hits through the Multitude of Structural Classes. Int J Mol Sci 2023;24:11518. https://doi.org/10.3390/ijms241411518.
46. Al-Nema M, Gaurav A, Lee VS. Docking based screening and molecular dynamics simulations to identify potential selective PDE4B inhibitor. Heliyon 2020;6:e04856. https://doi.org/10.1016/j.heliyon.2020.e04856.
47. Lai H, Wang L, Qian R, et al. Interformer: an interaction-aware model for protein-ligand docking and affinity prediction. Nat Commun 2024;15:10223. https://doi.org/10.1038/s41467-024-54440-6.
48. Chibuye B, Singh IS, Chimuka L, et al. In silico molecular docking, molecular dynamics, and ADMET analysis of metabolites from Strychnos cocculoides as potential therapeutics for erectile dysfunction: a comparative study with sildenafil. Discov Chem 2026;3:196. https://doi.org/10.1007/s44371-026-00656-y.
49. Abbasi M, Mansourian M, Oskouie AA, et al. In-silico study MM/GBSA binding free energy and molecular dynamics simulation of some designed remdesivir derivatives as the inhibitory potential of SARS-CoV-2 main protease. Res Pharm Sci 2024;19:29–41. https://doi.org/10.4103/1735-5362.394818.
50. Gilson MK, Stewart LE, Potter MJ, et al. Rapid, Accurate, Ranking of Protein–Ligand Binding Affinities with VM2, the Second-Generation Mining Minima Method. J Chem Theory Comput 2024;20:6328–40. https://doi.org/10.1021/acs.jctc.4c00407.
51. Sadashivanavar V, Madalageri M, Kinnal R, et al. Computational identification of marine-derived inhibitors of Cyclophilin D and Protease-Activated Receptor-1 for the treatment of ischemic disease. Journal of Molecular Graphics and Modelling 2026;145:109329. https://doi.org/10.1016/j.jmgm.2026.109329.
52. Zoete V, Irving MB, Michielin O. MM–GBSA binding free energy decomposition and T cell receptor engineering. Journal of Molecular Recognition 2010;23:142–52. https://doi.org/10.1002/jmr.1005.
53. Banerjee P, Kemmler E, Dunkel M, et al. ProTox 3.0: a webserver for the prediction of toxicity of chemicals. Nucleic Acids Res 2024;52:W513–20. https://doi.org/10.1093/nar/gkae303.
54. Abchir O, Rossafi B, Bouribab A, et al. In Silico Design of Pyrimidine Derivatives as Potential α-Glucosidase Inhibitors: QSAR, Molecular Docking, ADMET, and Molecular Dynamics Studies. International Journal of Molecular Sciences 2026;27:5696. https://doi.org/10.3390/ijms27135696.
55. Rajiv Gandhi G, Sharanya CS, Jayanandan A, et al. Multitargeted molecular docking and dynamics simulation studies of flavonoids and volatile components from the peel of Citrus sinensis L. (Osbeck) against specific tumor protein markers. Journal of Biomolecular Structure and Dynamics 2024;42:3051–80. https://doi.org/10.1080/07391102.2023.2212062.
56. Chalichem NSS, Jupudi S, Yasam VR, et al. Dipeptidyl peptidase-IV inhibitory action of Calebin A: An in silico and in vitro analysis. J Ayurveda Integr Med 2021;12:663–72. https://doi.org/10.1016/j.jaim.2021.08.008.

57. Ling C, Zhang X, Li X, et al. Molecular Simulations of Interface-Driven Crosslinked Network Formation and Mechanical Response in Composite Propellants. Polymers 2025;17:1863. https://doi.org/10.3390/polym17131863.
58. Singh M, Haque MdA, Tikhomirov AS, et al. Computational and Biophysical Characterization of Heterocyclic Derivatives of Anthraquinone against Human Aurora Kinase A. ACS Omega 2022;7:39603–18. https://doi.org/10.1021/acsomega.2c00740.
59. Evtyugin DD, Evtuguin DV. A comprehensive DPPH study on the antioxidant activity of ellagic acid from Eucalyptus sulphite pulping liquor for food applications. Food and Bioproducts Processing 2025;154:350–8. https://doi.org/10.1016/j.fbp.2025.10.005.
60. Baliyan S, Mukherjee R, Priyadarshini A, et al. Determination of Antioxidants by DPPH Radical Scavenging Activity and Quantitative Phytochemical Analysis of Ficus religiosa. Molecules 2022;27:1326. https://doi.org/10.3390/molecules27041326.
61. Gulcin İ, Alwasel SH. DPPH Radical Scavenging Assay. Processes 2023;11:2248. https://doi.org/10.3390/pr11082248.
62. Kumar A, Kaushik P, Incerpi S, et al. Evaluation of the Free Radical Scavenging Activities of Ellagic Acid and Ellagic Acid Peracetate by EPR Spectrometry. Molecules 2021;26:4800. https://doi.org/10.3390/molecules26164800.
63. Ramos-Torrecillas J, González-Acedo A, Melguizo-Rodríguez L, et al. Anti-Inflammatory and Antimicrobial Effect of Ellagic Acid and Punicalagin in Dermal Fibroblasts. Int J Mol Sci 2025;26:8681. https://doi.org/10.3390/ijms26178681.
64. da Silva BAF, Pessoa RT, da Costa RHS, et al. Evaluation of the antiedematogenic and anti-inflammatory properties of Ximenia americana L. (Olacaceae) bark extract in experimental models of inflammation. Biomedicine & Pharmacotherapy 2023;166:115249. https://doi.org/10.1016/j.biopha.2023.115249.
65. Arab HH, Gad AM, Fikry EM, et al. Ellagic acid attenuates testicular disruption in rheumatoid arthritis via targeting inflammatory signals, oxidative perturbations and apoptosis. Life Sci 2019;239:117012. https://doi.org/10.1016/j.lfs.2019.117012.
66. Wu M, Jiang Y, Wang J, et al. The Effect and Mechanism of Corilagin from Euryale Ferox Salisb Shell on LPS-Induced Inflammation in Raw264.7 Cells. Foods 2023;12:979. https://doi.org/10.3390/foods12050979.
67. Nourian YH, Salimian J, Ahmadi A, et al. cAMP-PDE signaling in COPD: Review of cellular, molecular and clinical features. Biochem Biophys Rep 2023;34:101438. https://doi.org/10.1016/j.bbrep.2023.101438.
68. Ko W-C, Shih C-M, Lai Y-H, et al. Inhibitory effects of flavonoids on phosphodiesterase isozymes from guinea pig and their structure–activity relationships. Biochemical Pharmacology 2004;68:2087–94. https://doi.org/10.1016/j.bcp.2004.06.030.